A Full Scale Elliptic CFD Analysis of the Anisotropic Flow in the Wake of a Wind Turbine

A. Herszage*, Y. Feldman
Dept. of Development of Energy Technologies,
Planning, Development & Technologies Div.
Israel Electric
P.O. Box 10, 31000, Haifa, Israel

Abstract

A full scale CFD elliptic analysis of anisotropic flow in the wake of a wind turbine was carried out. Special techniques of grid refinement were developed in order to provide accurate pressure and velocity distributions in the vicinity of the turbine blades and to ensure overall convergence and stability of the numerical solution. An acceptable qualitative agreement with previous numerical and experimental studies was obtained. The proposed model implementation requires no extra features other than those available in a commercial code, and may be a powerful instrument for wind turbine engineers.

Keywords: Wake; Turbulence; Anisotropy; CFD Elliptic analysis

* Corresponding author: amiel@iec.co.il ; Tel: 972-4-8183709, Fax: 972-4-8183723

Nomenclature

D- diameter of the turbine rotor

p- pressure

p_a- ambient pressure

$\boldsymbol{r}$- position vector

u_j- mean velocity component in the j direction

u'_j - fluctuating velocity component in the j direction

U_0- inlet incident wind velocity value

I_j- turbulence intensity component in the j direction, $I_j = u'_j / U_0$

$\boldsymbol{u}$- velocity vector

$\boldsymbol{u_r}$- relative velocity vector

x, y, z- Cartesian coordinates

ε_{ijk}- permutation operator

δij- Kronecker delta

Ω_k - rotation velocity component in the k direction

$\boldsymbol{\Omega}$– rotation velocity vector

μ- dynamic viscosity

ρ- density

y^+- friction dimensionless distance from the wall

ω- vorticity magnitude

1. INTRODUCTION

A continuing demand for electric energy and the environmental damage caused by conventional electrical generation has motivated an active search and promotion of renewable clean energy sources. Wind energy is in adequate conditions, one of the most effective means of environmental friendly electrical production. In this case wind turbines are used to convert the flowing air kinetic energy into electrical energy. Extracting the air flow energy, leads to significant modifications of the air flow field downstream the turbine rotor, resulting in a wake characterized by reduced mean velocity and static pressure.

A main momentum transfer mechanism from the fast external flow to the resulting slow flow downstream the rotor, is responsible for the wake structure and therefore for velocity recovery in the wind direction. Blade tip vortices created by blade motion in the viscous surrounding media, are shed downstream. They roll up in a short distance and move farther in helical trajectories (Gomez- Elvira et al, 2005). This behavior can be approximated by a cylindrical shear layer, which separates the slow moving fluid in the wake from the fast moving fluid outside (Sørensen and Shen, 2002). Momentum diffusion from this layer inwards in the downstream direction, results in wake diameter decrease with the consequent velocity recovery and turbulent energy transfer.

The above issue is of cardinal importance regarding wind farm design. An ideal arrangement of wind turbines should not be subjected to their mutual interaction. However, in regular arrays, downstream turbines are influenced by the wakes from the upstream rotors. This influence results in velocity deficits and increased levels of incident turbulence for the downstream turbines, leading to significant reduction in power production and unsteady loads increase. Unfortunately, these problems are difficult to avoid, since the areas suitable for wind energy production are limited. Hence, in order to ensure economical attractiveness of wind power generation, the wind turbines have to be assembled in arrays, inevitably leading to mutual wake interactions. In this respect significant energy losses have been measured in arrays spaced at less than seven turbine diameters (Crespo et al, 1999). As a result, optimization of wind turbines layout in wind farms has been a subject of extensive study over the recent three decades. This subject is briefly described below, in order to focus on the purpose of this work. Experimental findings within this large group of investigations have provided the main motivation for the present work. These experimental observations concern turbines arranged in line (Vermeer et al, 2003; van Leuven and Stevens, 1988). According to them, while the first turbine produces full power, there is a significant decrease of power in the second turbine, with practically no further loss in successive machines. On this basis, it is proposed to use a straightforward approach, using a commercial finite volume code (Fluent, 2001) for the numerical solution of the fully anisotropic flow field, including direct rotor modeling. In terms of reasonable computational resources available at the present time, the full modeling of the flow field around a small number of turbines is not out of reach. As a first step towards this goal, it is necessary to validate and fully

understand the limitations and results of such an approach for a single turbine, presented in this work.

A pioneering theoretical model estimating wind power extraction efficiency of arbitrary wind turbines arrays was proposed by Lissaman (1979). The author assumed linear superposition of the perturbations created by the wakes of different turbines. However, this simplified assumption fails for large perturbations, overestimating the velocity deficits and leading to non physical negative values of velocities for large number of superimposed wakes (Vermeer et al, 2003). To overcome this problem, Katic et al. (1986) assumed linear superposition of the velocity deficits squares. Although the assumption provides much better agreement with experimental results in comparison with the linear superposition of velocity deficits, its physical validity is not completely obvious (Vermeer et al, 2003). Smith and Taylor (1991) presented both experimental and analytical studies of wake interactions, generated by two machines when one turbine was placed directly downstream the other. The experiments showed that the wake immediately behind the downstream machine recovered along a shorter path than that behind the upstream machine. The implemented scheme uses a kinematic assumption regarding the transverse direction. This semi empirical approach renders good agreement was found between the predicted and measured mean velocity profiles at all downstream distances.

The study of wind power extraction efficiency from a turbine array was consequently extended by a set of experimental works (van Leuven and Stevens, 1988; Beyer et al, 1994; Corten et al, 2004), which investigated the wake flow distribution characteristics and the power generated by a large number of turbines located in line. As mentioned above, their main conclusion was that while the first turbine produces full power, there is a significant decrease of power in the second turbine with practically no further loss in successive turbines.

The same conclusion regarding power production of a number of turbines arranged in line was reached by Crespo et al. (1990, 1994). At their earlier study (Crespo et al, 1990), the authors applied a fully elliptic model to investigate the interaction of the wakes originated behind two turbines located in line. Further simplification led to the parabolic computer code UPMPARK for the case of a park with many machines (Crespo et al, 1994). This simplification was justified by the fact that the length of the typical wake is much larger than its width, which renders predominating transverse momentum diffusion over the longitudinal one. According

to the authors, the truly elliptic effects, i.e. second order derivatives of all velocity components in the axial direction prevail only in close vicinity of the turbine rotor and therefore may be safely neglected over most of the wake interactions domain. Though the idea is clearly time saving motivated, independent implementation of the parabolic equations and the specifically developed turbulence model require extensive programming efforts.

The interaction of several wakes in double and quintuple wake cases was comparatively studied within the ENDOW project (Schlez et al, 2001; Barthelmie et al, 2004; Rados et al, 2001). In the case of low ambient turbulence (6%) all the models overestimated velocity deficits in comparison with experimental data. Higher accuracy was obtained in the case of higher ambient turbulence (8%). Moreover, both theoretical and experimental studies showed very moderate deviations between the corresponding velocity deficits of double and quintuple wakes. These findings confirm the above mentioned conclusions, regarding small power output differences between the second turbine and those arranged successively downstream (van Leuven et al, 1988; Beyer et al, 1994; Corten et al, 2004; Crespo et al, 1990; Crespo et al, 1994).

It is important to notice that despite the substantial improvement of wake interaction models within the past few years, there are still discrepancies between the majority of the models and the experimental data regarding flow characteristics (Schlez et al, 2001; Barthelmie et al, 2004; Rados et al, 2001). Most of them have been tested for assumptions and coefficients chosen to fit particular experimental data. Therefore, the aspect of their overall validity is still problematic (Katic et al, 1986). In this respect, improvement of multiple wake studies, can be based on further exploration and improvement of single wake calculations. Magnusson et al. (1996) investigated the characteristics of the flow at near and far wakes of a wind turbine, using an axisymmetric solver for the turbulent Navier-Stokes equations in the near wake. Clearly by enforcing such symmetry assumption, limitations are enforced on the different velocity spatial distributions. The velocity field in the far wake was calculated assuming that the air flow is fully developed and characterized by self preservation profiles. The study was followed by more sophisticated numerical models based on CFD calculations to estimate the turbine power (Bak et al, 1999), on BEM theory to obtain the near wake characteristic (Magnusson, 1999) and on

boundary layer approximation to analyze the bi-dimensional shear layer at the near wake (Crespo and Hernandez, 1996).

Recently a parabolic model was developed (Gomez- Elvira et al, 2005) to study the non-isotropic characteristics of turbulence in wind turbine wakes. The authors developed a calculation method based on an explicit algebraic model for the components of the turbulent stress tensor. As expected, isotropic turbulence was obtained in the vicinity of the wake center, while peaks of turbulence production were observed in the shear layer of the wake. This model assumes an inlet boundary condition for a disk equivalent to the rotor outlet and its surrounding plane.

The purpose of the present study is to perform a straight forward, full scale analysis on a 500 kW wind turbine. This is done by evaluating air flow characteristics at every point in the flow field without making any preliminary assumptions neither about the final wake geometry, nor about the flow field immediately downsream the rotor. Most of the study is based on data from a NedWind 46/3/500 turbine. The study was performed using a commercial CFD finite volume software package (Fluent, 2001). Reasonable agreement was obtained with respect to manufacturer's data (turbine power output- wind speed values). A fully anisotropic RANS (Reynolds Averaged Navier- Stokes) treatment is used, and the rotor geometry is introduced directly without any previous assumptions. The approach proposes a simple and powerful engineering tool for wind turbines design evaluations, as well as for enhancing performance of wind farms. As mentioned above, this work intends to provide a clear view of the capabilities and limitations of this approach for a single turbine. The ideas leading to its expansion, for its use as a wind farm design tool, are based on the further solution of the flow field for a limited number of turbines and the use of experimental findings (van Leuven and Stevens, 1988; Beyer et al, 1994; Corten et al, 2004) concerning the repeatability of flow features.

2. THE MODEL

2.1 Turbine geometry and computational domain

A schematic picture of the wind turbine analyzed in the present work is shown in Fig.1. The turbine has a 46 meters rotor diameter and consists of three equal blades positioned at 120º relative to each other. The wind turbine hub and nacelle were also modeled. The blades are built from sections characterized by a variable twist angle (chord- rotation plane angle) varying from 12º at the hub vicinity to 0º at the blade

edge. The turbine hub is positioned at 40 meters height. Although the real NedWind turbine has a tilt angle of 5º between the rotor and the *y-z* plane (see Fig. 2- clockwise around the y axis), the analysis performed in this study assumed that both planes are parallel. This assumption eliminated the need to address the wake-ground collision problem, enabling at this stage for a thorough investigation of the model capabilities to describe the physics of the wake.

The computational domain and the position of the wind turbine relatively to the domain boundaries are shown in Fig. 2. Though no particular limitations are imposed by the implemented approach, the influence of the turbine tower is neglected at this stage, in order to simplify the geometrical complexity of the problem. As indicated in Fig. 2, the Cartesian coordinates system (*x*,*y*,*z*) is attached to the geometrical center of the back of the turbine hub while the *x-y* plane is parallel to the lower boundary (ground). Two turbine diameters separate between the rotor center and the lateral boundaries of the domain, while 3.5 diameters separate between the hub center height and the domain upper boundary. The distance between the turbine center and downstream boundary is equal to twelve turbine diameters. The upstream inlet is located at a distance equal to two diameters from the rotor plane. These distances should provide a fully developed air flow in the vicinity of upstream (Corten et al, 2004) downstream (Rados et al, 2001), upper and lateral (Magnusson, 1999) boundaries of the computational domain.

2.2 Computational mesh

The computational domain discretization was realized by using a mixed three dimensional mesh. At a first stage the whole domain was separated into twelve volumes (see Fig. 3), ten of which (from 1 to 10) were meshed with structured brick cells. Volume 11, representing a rectangular prism with a subtracted cylinder at its center, was meshed with unstructured tetrahedral cells and rectangular pyramids at its outer layer, which are connected to the above mentioned bricks. Finally, the mesh generation of volume 12 comprising a cylinder with the subtracted blades, hub and nacelle of the wind turbine is performed as described below. Fig. 4 presents a detailed sketch of a typical mesh structure at a section adjacent to the turbine blade. All blade surfaces were meshed using quadrilateral structured cells which were used as a basis for the boundary layer structure adjacent to the blades. The structure consists of a

sequence of 5 layers characterized by a first layer thickness of 2 millimeters and growth ratio of 1.2, having an overall thickness of about 15 mm. After a number of numerical simulations, such configuration was revealed as optimal, providing proper flow characteristics at the blade vicinity and efficient memory use. The boundary layer is followed by a mixed cell mesh, evolving from rectangular pyramids to tetrahedrons. This procedure ensures a smooth transition outward the blades vicinity region, at which viscous forces are dominant.

Another boundary layer structure consisting of a sequence of 10 layers with a first layer thickness of 100 millimeters and a growth ratio of 1.2 was attached to the domain bottom (ground) surface (z= 0.87.D, see Fig. 2). For both boundary layers the y^+ function values along the bottom surface and all turbine blades were in the range of $y^+ \in$ [30, 300]), indicating that the obtained solution satisfies the implemented standard wall functions requirements (Fluent, 2001).

After a number of numerical simulations it was revealed that the largest pressure gradients along the whole blade occur in the vicinity of its leading edge. Therefore the computational grid at this region was generated with larger density in comparison with other regions adjacent to the turbine blade (see Fig. 4). In order to validate the numerical solution, the turbine power at the operating angular velocity was calculated and numerical convergence was verified. The above rationale was realized by computing the moment vector acting on the turbine blades directly within the CFD program. The calculation was realized using a moving reference computational scheme described below. The turbine power at the operating angular velocity was then calculated and the leading edge grid density increased until the relative wind turbine power deviation between the two adjacent mesh configurations was less than 1%, in order to ensure numerical convergence. Throughout the simulations the blade surface was assumed to be smooth. The influence of blade surface roughness and the effects of vortex generators present in the blade were therefore not included at this stage. Experimental evidence (Fuglsang et al, 1998) indicates that vortex generators and relatively small increases in surface roughness, could lead to a significant increase of the driving moment (up to 15 % in some cases). These effects are a result of the differential pressure distribution on the blade, caused by chord wise extension of the non separated boundary layer on the suction side of the airfoil. Considering the deviations due to the above mentioned effects, the overall deviation between the power produced by the real turbine without vortex generators and that obtained by the

CFD simulation would not exceed 13%, denoting a reasonable agreement between the experimental and the numerical results.

The overall number of cells was of the order of $5x10^6$. Special attention was given to keeping the mesh skewness values within a reasonable range, in order to obtain a reliable solution at every point of the computational domain.

2.3 Governing equations and boundary conditions

The air flow around the wind turbine was supposed to be steady, incompressible and gravitational effects neglected. Neutral atmospheric conditions were implemented by assuming suitable values of the inlet wind velocity and turbulence intensity. Therefore the energy equation is not solved in the applied scheme. The treatment of turbulence was realized by using the Reynolds-averaged approach leading to the Reynolds-averaged Navier-Stokes (RANS) equations. In this case the continuity and linear momentum equations, respectively, can be written in Cartesian tensor form as:

$$\frac{\partial u_i}{\partial x_i} = 0 \qquad (1)$$

$$u_j \frac{\partial u_i}{\partial x_j} = -\frac{1}{\rho}\frac{\partial p}{\partial x_i} + \frac{\mu}{\rho}\frac{\partial}{\partial x_j}\left(\frac{\partial u_i}{\partial x_j}\right) + \frac{\partial}{\partial x_j}\left(-\overline{u_i' u_j'}\right)$$

where the index values of i, j = 1,2,3 correspond to Cartesian coordinates (x,y,z), u_i and u_i' are respectively the mean and the fluctuating velocity components, ρ is the air density, μ is the air dynamic molecular viscosity and $\overline{u_i' u_j'}$ are the time averaged products of the fluctuating velocity components, known also as Reynolds stresses.

The additionally introduced unknowns, i.e. the Reynolds stresses, represent in the system of equations (1) six additional unknown terms which must be modeled. A frequently used method for Reynolds stresses modeling is based on the eddy-viscosity (Boussinesq) hypothesis (Hinze, 1995), which assumes the turbulent viscosity as an isotropic scalar magnitude. Clearly, the anisotropy of the turbulent stress components responsible for the structure of the wake cannot be properly reproduced by isotropic models (Gomez- Elvira et al, 2005). In light of the above mentioned limitations, an anisotropic turbulence model, available in commercial CFD codes (Fluent, 2001) was used in this work. This model is known as the Reynolds stresses model (RSM). The

RSM model closes the RANS equations (1) by using exact transport equations for the individual Reynolds stresses, $\overline{u_i' u_j'}$:

(2)

$$\underbrace{\frac{\partial}{\partial x_k}\left(u_k \overline{u_i' u_j'}\right)}_{C_{ij} \equiv \text{Convection}} = \underbrace{-\frac{\partial}{\partial x_k}\left[\overline{u_i' u_j' u_k'} + \overline{\frac{p}{\rho}\left(\delta_{kj} u_i' + \delta_{ik} u_j'\right)}\right]}_{D_{T,ij} \equiv \text{Turbulent Diffusion}} + \underbrace{\frac{\partial}{\partial x_k}\left[\frac{\mu}{\rho}\frac{\partial}{\partial x_k}\left(\overline{u_i' u_j'}\right)\right]}_{D_{L,ij} \equiv \text{Molecular Diffusion}}$$

$$\underbrace{-\left(\overline{u_i' u_k'}\frac{\partial u_j}{\partial x_k} + \overline{u_j' u_k'}\frac{\partial u_i}{\partial x_k}\right)}_{P_{ij} \equiv \text{Stress Production}} + \underbrace{\overline{\frac{p}{\rho}\left(\frac{\partial u_i'}{\partial x_j} + \frac{\partial u_j'}{\partial x_i}\right)}}_{\phi_{ij} \equiv \text{PressureStrain}} - \underbrace{2\frac{\mu}{\rho}\overline{\frac{\partial u_i'}{\partial x_k}\frac{\partial u_j'}{\partial x_k}}}_{\varepsilon_{ij} \equiv \text{Dissipation}}$$

$$\underbrace{-2\Omega_k\left(\overline{u_j' u_m'}\varepsilon_{ikm} + \overline{u_i' u_m'}\varepsilon_{jkm}\right)}_{F_{ij} \equiv \text{Production by System Rotation}}$$

Unfortunately, several of the terms in the exact equations (i.e. $D_{T,ij}$, ϕ_{ij}, ε_{ij}) are unknown (notice the triple products, single velocity fluctuation derivatives, etc., while the double products constitute the unknowns of the problem). Therefore, modeling assumptions are required to attain closure of the equations.

Following the above rationale, the turbulent diffusion, $D_{T,ij}$ is modeled using a scalar turbulent diffusivity as follows (Lien and Leschziner, 1994):

$$D_{T,ij} = \frac{\partial}{\partial x_k}\left(\frac{\mu_t}{\sigma_k}\frac{\partial \overline{u_i' u_j'}}{\partial x_k}\right) \qquad \text{(2-a)}$$

The value of $\sigma_k = 0.82$ in the above equation, was derived by applying the generalized gradient- diffusion model (Daly and Harlow, 1970) to the case of a planar homogeneous shear flow. The turbulent viscosity, μ_t, is computed as:

$$\mu_t = \rho C_\mu \frac{k^2}{\varepsilon} \qquad \text{(2-b)}$$

The adopted value of $C_\mu = 0.03$ was proposed by Magnusson (1996). The turbulence kinetic energy, k, necessary for the equivalent turbulent viscosity (2-b), is computed by calculating half of the trace of the Reynolds stress tensor, $k = 1/2\,\overline{u_i' u_i'}$ and the scalar dissipation rate, ε, is computed by means of a steady model transport equation:

$$\rho\frac{\partial}{\partial x_i}(\varepsilon u_i)=\frac{\partial}{\partial x_j}\left[(\mu+\mu_t)\frac{\partial\varepsilon}{\partial x_j}\right]+\frac{1}{2}\frac{\varepsilon}{k}C_{\varepsilon 1}P_{ii}-C_{\varepsilon 2}\rho\frac{\varepsilon^2}{k} \qquad (2\text{-c})$$

where $C_{\varepsilon 1}$ = 1.44, and $C_{\varepsilon 2}$ = 1.92. Regarding the values assumed for the turbulence model constants, except for C_μ, the rest of them were assumed at this stage as the default values given in the software package (Fluent, 2001).

This study utilizes the classical approach for the pressure strain term, ϕ_{ij}, (Fluent, 2001) using the following decomposition:

$$\phi_{ij}=\phi_{ij,1}+\phi_{ij,2}+\phi_{ij,w} \qquad (2\text{-d})$$

where $\phi_{ij,1}$ is the slow pressure strain term, also known as the return-to-isotropy term, $\phi_{ij,2}$ is called the rapid pressure strain term, and $\phi_{ij,w}$ is the wall-reflection term. The slow pressure strain term, $\phi_{ij,1}$, is modeled as:

$$\phi_{ij,1}=-C_1\rho\frac{\varepsilon}{k}\left[\overline{u_i'u_j'}-\frac{2}{3}\delta_{ij}k\right] \qquad (2\text{-e})$$

with C_1= 1.8 (Fluent, 2001). The rapid pressure-strain term, $\phi_{ij,2}$, is modeled as:

$$\phi_{ij,2}=-C_2\left[\left(P_{ij}+F_{ij}-C_{ij}\right)-\frac{2}{3}\delta_{ij}(P-C)\right] \qquad (2\text{-f})$$

where C_2 = 0.6, P_{ij}, F_{ij}, and C_{ij} are defined as in Eq. (2), $P = 1/2P_{kk}$ and $C = 1/2C_{kk}$. The wall-reflection term, $\phi_{ij,w}$, is responsible for the redistribution of normal stresses near the wall. It tends to damp the normal stress perpendicular to the wall, while enhancing the stresses parallel to the wall. This term is modeled as:

$$\phi_{ij,w}=C_1'\frac{\varepsilon}{k}\left(\overline{u_k'u_m'}n_kn_m\delta_{ij}-\frac{3}{2}\overline{u_i'u_k'}n_jn_k-\frac{3}{2}\overline{u_j'u_k'}n_in_k\right)\frac{k^{3/2}}{C_l\,\varepsilon\,d}+ \qquad (2\text{-g})$$

$$+C_2'\left(\phi_{km,2}n_kn_m\delta_{ij}-\frac{3}{2}\phi_{ik,2}n_jn_k-\frac{3}{2}\phi_{jk,2}n_in_k\right)\frac{k^{3/2}}{C_l\,\varepsilon\,d}$$

where the values of $C_1^{'} = 0.5, C_2^{'} = 0.3$, have been adopted (Fluent, 2001). n_k is the x_k component of the unit normal to the wall, d is the normal distance to the wall, and $C_l = C_\mu^{3/4} / k$, where C_μ = 0.03 and k is in this case the von Kármán constant (k= 0.4187). The dissipation tensor ε_{ij} (see eq. 2), is modeled as follows:

$$\varepsilon_{ij} = \frac{2}{3}\delta_{ij}\rho\varepsilon \qquad \text{(2-h)}$$

As may be seen, the above equations, which model the $D_{T,ij}$, ϕ_{ij}, ε_{ij} terms, contain a number of constants. Their values have been chosen on the basis of experiments for given conditions (Fluent, 2001). Clearly, these conditions are not necessarily similar to those of the particular problem in question. Therefore, while this turbulence modeling approach renders a fully anisotropic solution, its accuracy can be compromised by the model assumptions. The evaluation and exact fitting of these constants would require extensive experimental and numerical work, which is beyond the scope of the present study.

The appropriate no slip and no penetration boundary condition for the velocity at the stationary bottom boundary (z= 0.87D, see Fig. 2) is:

$$\boldsymbol{u}\left(x, y, z = 0.87D\right) = 0 \qquad (3)$$

At the vicinity of lateral and top boundaries (see Fig. 2) the air flow is supposed not to be affected by the turbine presence (Magnusson, 1999). Therefore, symmetry boundary conditions were applied at these boundaries, namely:

$$\begin{aligned} &u_y\left(x, y = 2D, z\right) = u_y\left(x, y = -2D, z\right) = u_z\left(x, y, z = -3.5D\right) = 0 \\ &\frac{\partial \Phi}{\partial y}\left(x, y = 2D, z\right) = \frac{\partial \Phi}{\partial y}\left(x, y = -2D, z\right) = \frac{\partial \Phi}{\partial z}\left(x, y, z = -3.5D\right) = 0 \end{aligned} \qquad (4)$$

where Φ is related to any physical unknown represented by the governing equations (1) and (2). The corresponding velocity inlet and pressure outlet boundary conditions are assumed as fully developed flow conditions (Corten et al, 2004; Rados et al, 2001) (see Fig. 2):

$$u_x\left(x = -2D, y, z\right) = U_0 \quad \text{and} \quad p\left(x = 12D, y, z\right) = p_a \qquad (5)$$

U_0 = 10 m/sec represents the mean component of the air inlet velocity and p_a the ambient pressure. The turbine operating angular velocity is 28.5 rpm determining the turbine blades velocity boundary condition as:

$$\Omega(blades) = 2.98\hat{e}_x \, rad/\sec \qquad (6)$$

$\hat{e}_x$ represents the unit direction vector of the *x* axis (see Fig. 2).

The isotropic turbulent flow at the upstream boundary of the domain, allows for the use of turbulence intensity, I (10% was assumed) and hydraulic diameter, D_H method for specifying the turbulence dissipation rate ε and the individual Reynolds stresses $\overline{u_i' u_j'}$ at the flow inlet, necessary for the RSM model implementation as follows:

$$\varepsilon = C_\mu^{3/4} \frac{k^{3/2}}{l} \qquad (7\text{-a})$$

$$\overline{u_i' u_j'} = \frac{2}{3} k \delta_{ij} \qquad (7\text{-b})$$

The turbulent kinetic energy, k is related to the inlet air velocity, U_0 and the turbulence intensity, I at the inlet boundary by $k = 3/2(U_0.I)^2$, whereas the turbulence length scale l is expressed in terms of hydraulic diameter D_H as $l = 0.07D_H$. At all other boundaries the Reynolds stresses and the dissipation rates were obtained explicitly by using wall functions and assuming equilibrium, disregarding convection and diffusion in the transport equations (2) as was detailed in the given reference (Fluent, 2001).

2.4 The solution procedure

Due to the rotor blades sweeping the domain periodically, the fluid motion is unsteady in the ground attached domain. Nevertheless, the mean properties of the wake structure can be studied using a steady state approach. Hence, in the present study the wind turbine rotation was modeled utilizing a steady state single rotating frame approach [ ]. The computational domain, see Fig.3 was subdivided into rotating (volume 12) and static (the rest of domain) sub-domains. Notice that the flow inside the rotating volume is steady with respect to the non inertial frame, attached to volume 12, which greatly simplifies the analysis. The air flow may then be expressed either in terms of absolute, $\boldsymbol{u}$, or relative $\boldsymbol{u}_r$ velocities related to each other by:

$$\boldsymbol{u} = \boldsymbol{u}_r + (\boldsymbol{\Omega} \times \boldsymbol{r}) \tag{8}$$

where $\boldsymbol{\Omega}$ is the rotor angular velocity vector, i.e. the rotational velocity of the rotating frame, and $\boldsymbol{r}$ is the position vector in the rotating frame.

After substitution of the above equation, the RANS equations (1) are rendered in terms of relative velocity $\boldsymbol{u}_r$, representing the air flow field inside the rotating sub-domain and may be written in vector form as:

$$\begin{gathered} \nabla \bullet \boldsymbol{u}_r = 0 \\ (\boldsymbol{u}_r \bullet \nabla)\boldsymbol{u}_r + (2\boldsymbol{\Omega} \times \boldsymbol{u}_r + \boldsymbol{\Omega} \times \boldsymbol{\Omega} \times \boldsymbol{r}) = -1/\rho \nabla p + \mu/\rho \nabla^2 \boldsymbol{u}_r + \nabla \bullet \left(\overline{\boldsymbol{u}' \boldsymbol{u}'}\right) \end{gathered} \tag{9}$$

The exact transport equations for the individual Reynolds stresses (2) may be also expressed in terms of the relative velocity $\boldsymbol{u}_r$ (Fluent, 2001). The procedure is omitted here for the sake of brevity.

A segregated solution approach was used to solve the governing equations (Fluent, 2001). The SIMPLE algorithm, using the relationship between velocity and pressure correction was utilized to enforce mass conservation and to obtain the pressure field. Domain reordering using the reverse Cuthill-McKee method was applied in order to minimize computer memory requirements.

3. RESULTS AND DISCUSSION

3.1 Wake flow analysis

The full scale spatial kinematical behavior of the air flow in the turbine wake can be understood from Fig. 5, representing iso-curves of the velocity component in *x* direction. As expected from disk rotor theory the upstream wind velocity slows down just before the rotor disc (see Fig. 5a and 5b). The presence of the ground at the bottom of the computational domain has a significant effect on the air flow in the turbine wake, which is characterized by a distinct downward slope in the downstream flow direction, as may be seen from Fig. 5a. This is because the wake recovery rate caused by the wake interaction with the external flow is considerably smaller in the ground vicinity than in the rest of the domain.

In addition to the downward slope, the wake is also characterized by its downstream deflection in the negative direction of the *y* axis, as it is shown in Fig. 5b.

Such behavior is explained by the angular momentum conservation principle, imparting to the air that has just passed the turbine rotor an angular velocity opposite to that of the turbine blades rotation.

Furthermore, it can be seen from Fig. 5 that there is an extensive region, immediately downstream the rotor, around the rotor perimeter, which shows higher values of the *x* velocity than the inlet flow velocity values. This is in agreement with the continuity law, providing the same mass flow rate at each cross section of the domain. The larger velocity region is extended in the $(-\hat{y})$ and $(-\hat{z})$ directions, as a result of the ground presence and the angular velocity of the turbine wake.

3.2 Vorticity analysis

Significant variation in air flow circulation along the turbine blades leads to vortex sheets generation, which are shed from the blades trailing edge and roll up within a short downstream distance, forming tip vortices that describe helical trajectories (Crespo et al, 1999). These vortices leads to a shear layer formation, separating between the free and wake flows. Turbulent diffusion results in the increase of the shear layer thickness with downstream distance, reaching at a certain downstream distance the wake axis. This marks the end of the near wake region. A full scale vorticity analysis was performed to investigate the shear layer expansion. Additionally, its results determine the location of the transition region between the near and the far wakes. Fig.6 shows the vorticity distribution in the mid horizontal cross section of the computational domain. Maximum vorticity values of 0.17 rad/sec were found along the outer perimeter of the wake and also directly behind the turbine rotor close to the turbine blades tips and hub. While the first observation was expected from the rotor disk theory, the second one may be obtained only by the CFD calculations and probably is a consequence of flow instabilities in the vicinity of the hub. The vorticity values decrease when advancing in the *x* and *y* directions as a result of turbulence diffusion. As may be seen from Fig. 6 the shear layer reaches the wake axis at about 7.5*D* downstream the turbine, denoting the end of the near wake region. Vorticity distribution in the mid vertical lengthwise section (x-z plane) was found very similar to that presented in Fig. 6, and therefore was not shown separately.

3.3 Velocity deficit analysis

It is common to express the wake recovery process, caused by its interaction with the external free flow, in terms of velocity deficit value, defined as a $(U_0\text{-}u_x)/U_0$. Figure 7a depicts the velocity deficit values at the top, hub and bottom heights of the rotor disc versus downstream distance from the turbine. Throughout the domain, the maximum values of the velocity deficit were obtained at the hub height. Along this axis there is insignificant increase in the velocity deficit values from x=2D to x=7.5D which then decrease rapidly up to x=12D. As was explained in the previous section, such behavior is a result of turbulent diffusion, leading to the shear layer thickness increase with downstream distance, which finally reaches the wake axis at x=7.5D.

The velocity deficit values at the top of the rotor disc are about twice less than the corresponding values at its bottom, indicating a significant effect of the ground at the bottom of a computational domain, which slows down the wake recovery rate.

Fig. 7b shows the velocity deficit distribution in the mid horizontal cross section (see x-y plane in Fig. 2) versus its offset from the hub axis, for five different downstream distances. It may be seen that the maximum values of the velocity deficit are located close to the hub axis and are almost the same for the downstream distances lying in the range of $2.5D \leq x \leq 7.5D$. Furthermore, when moving in $\pm y$ direction (see Fig.2) there is a substantial decrease of the velocity deficit values at this range of x, which moves inwards as the downstream distance increases. This phenomenon is explained by the shear layer expansion with the downstream distance, which for values of $x \leq 7.5D$ has not yet reached the hub axis. At x=10D and x=12D the shear layer has reached the hub axis, causing a steep decrease of the velocity deficit values in its vicinity. It should be noted that the near wake velocity deficit distribution ($x \leq 7.5D$) is not symmetric relatively to the hub axis. This is caused by the wake downstream deflection in the negative direction of the y axis (see Fig.2), as a result of the wake angular velocity.

As the downstream distance increases to x=10D and to x=12D, the velocity deficit distribution takes a more symmetric form relatively to the hub axis, owing to the dominant role of the air flow turbulence at the fully developed wake, were ambient shear flow may be assumed (Crespo et al, 1999). The velocity deficit distribution in the mid vertical lengthwise section for several downstream distances, which is shown in Fig. 7c, has similar shear layer characteristics to the one observed in the mid horizontal cross section. However, in this case, the asymmetric structure of

the velocity deficit distribution is clearly observed, almost throughout the whole range of downstream distances ($2.5D \leq x$), caused by the ground presence.

Particular attention has been given to validate the proposed numerical model in terms of the velocity deficit distribution. Unfortunately, experimental data regarding the velocity characteristics in the wake of the NedWind 46/3/500 turbine was not available at the time. Nevertheless, in order to ensure numerical validity of the results, a special grid refinement procedure was developed to prove the convergence and numerical stability of the solution. In order to overcome the computer memory limitations, the further analysis was performed only on the downstream computational sub-domain consisting of volumes 6- 8 (see Fig. 3) which contained approximately $2x10^6$ cells. At the inlet boundary of the new sub-domain, all velocity components and Reynolds stresses values obtained from the initial full domain solution, were used explicitly as inlet boundary conditions for the analysis. In order to verify repeatability of the scheme, the corresponding results obtained from the full and sub-domain analysis were then compared and found equal to each other. A further refinement of the computational sub-domain was achieved by dividing each cell were the vorticity value was in its typical range of $0.05 \text{ rad/sec} \leq \omega \leq 0.2 \text{ rad/sec}$ into eight equal sub-cells, resulting in an overall number of cells of approximately $5x10^6$. A comparison between the refined and unrefined solution revealed insignificant differences (no more than 5%) between the corresponding velocity deficits values, indicating that the obtained full scale solution is converged and numerically stable.

3.4 Turbulence analysis

The Reynolds stress model (RSM), used in this research, allows for the calculation of the Reynolds stresses as six independent variables. Their solutions are used herein to calculate the turbulence intensity and anisotropic properties of the flow. Figures 8a - 8c show respectively turbulence intensity distributions in the *x*, y and *z* directions at the near, transition and far wake regions of the turbine. It may be seen that for all three directions shown in Fig. 8 the near and the transition wake regions are characterized by turbulence intensity values which are close to each other in the inner region of the wake. This is a result of the clear tendency of the turbulence to be more isotropic in the core of the wake. At the same time in the far wake the turbulence intensity in the *x* direction (see Fig. 8a) is significantly larger than the

turbulence intensities in *y* and *z* directions, which in turn are very similar to each other (see Figures 8b and 8c).

Notice that in the far wake region (*12D*), far enough from the location where the shear layer reached the wake axis, the hub height turbulence intensity values in all directions are about 4.5 times larger than the corresponding values at the near and transition regions.

The distribution of the *x* component turbulence intensity in the transition and far wake regions is characterized by the peak values of turbulence intensity at about one turbine radius above the hub axis (see Fig. 8a) as was also reported in [12]. However this behavior is not observed on the transition and the far wake regions for the *y* and *z* components (see Fig. 8b- c), which are characterized by almost identical moderate values of turbulence intensities. The above is a manifestation of the anisotropic character of the turbulence in this problem. Notice that when moving up away from the wake axis the turbulent intensity value in all directions approaches that of the external flow, which is equal to 0.1.

The spatial distribution of the rate of momentum turbulent diffusion, between the external and wake flows was estimated by performing a dimensionless correlation analysis, shown in Fig. 9. Fig. 9a shows the dimensionless $\overline{u'_x u'_z}$ correlation (x-z plane) versus the distance from the hub axis in the near and far wakes. Both correlations get their maximum values at about one radius away from the hub axis in the near and far wakes. However, for the near wake correlation the maximum value peaks have a much steeper character than those obtained for the far wake. This fact is an indication of the small thickness of the near wake shear layer which then increases with downstream distance.

The near wake correlation is anti symmetric relatively to the hub axis at almost the whole computational domain excepting its bottom part where the symmetry is distorted as a result of ground presence. This result indicates uniform diffusion rate of momentum up and down the hub axis. The distortion introduced by the ground, becomes more noticeable in the far wake region, where the correlation values obtained below the turbine hub are approximately twice less than those obtained at the same distance above it.

Dimensionless correlation values of $\overline{u'_y u'_z}$ and $\overline{u'_x u'_y}$, shown respectively in Fig. 9b and Fig. 9c are one order of magnitude smaller than the corresponding

values of the $\overline{u'_x u'_z}$ correlation. Therefore, as expected, the largest amount of momentum imparted from the external flow to the wake flow in the *x*-*z* plane, proceeds in the *z* direction. Contrary to the $\overline{u'_x u'_z}$ distribution, the $\overline{u'_y u'_z}$ distribution is not anti symmetric relatively to the hub axis in the near wake. For example, the maximum value of the $\overline{u'_y u'_z}$ correlation is located one radius above the hub axis (see Fig. 9b). This value is larger than the corresponding value located one radius below the hub axis, suppressed by the ground presence. This is probably due to the azimuthal velocity gradient, which is naturally larger one radius above the axis, than one radius below it, where ground suppressing effects are expected. Different behavior in the near wake is observed for the $\overline{u'_x u'_y}$ correlation (see Fig. 9c), having its maximum value at about one radius below the hub axis. The reason for this behavior might be associated with the fact that in this case, momentum transfer through the shear layer is not enforced through the *xy* shear component, due to the very direction of the flow in the vicinity of the shear layer. Therefore, the xy component would be influenced by the free flow boundary layer velocity gradient which is stronger close to the ground.

A dimensionless correlation analysis for the near and far wakes was also performed in the mid horizontal cross section (x-y plane). For this case, as expected the $\overline{u'_x u'_y}$ values were found to be largest ones. As it can be seen the results in all cases indicate that the bulk of turbulent momentum is transferred from the free flow inwards through the shear layer along the direction of the wind. This statement is in agreement with the conclusion of both the experimental and numerical work of Smith and Taylor (1991) in which they reported about a well defined ring shaped region observed around a cylindrical shear layer, characterized by high turbulence intensity values.

4. CONCLUSIONS

A full scale CFD analysis was performed to investigate the wake characteristics of a NedWind 46/ 3/ 500 turbine in terms of velocity distribution. The model renders six components of the Reynolds stress tensor required to estimate the strongly anisotropic flow patterns characteristic of this problem. Turbulence intensity and the corresponding shear correlations, responsible for turbulent momentum transfer, at any

point of the computational domain are rendered by the model and examined in this work. It was found that the near wake is characterized by a more isotropic behavior than the far wake. Peaks of turbulence intensity were found on relevant locations along the shear layer. The model renders asymmetric wake geometry, as ground and angular momentum effects are inherently built within the solution. The effects of ground presence and the vorticity property on the wake structure were also studied. The model implementation requires no extra features other than those available in a commercial code, and may be a powerful instrument for wind turbine engineers.

Considerable efforts were invested in order to ensure numerical convergence. The implemented procedures rendered adequate boundary layer profiles both around the blades and on the ground. Moreover, the above mentioned profiles constitute a necessary condition for the computational verification of the power available on the rotor, performed within the work. Additional grid refinement, implemented in high vorticity zones was used in order to verify stable location of the shear layer and its expansion. In addition, the solution of the full problem was used as an input to an additional computation, performed on a subdomain after the rotor outlet was replaced by the equivalent numerical solution. The results obtained after a massive overall grid refinement of the region downstream the rotor confirmed the numerical accuracy of the full solution.

Features of the anisotropic turbulent field relevant for the structure of the wake, the shear layer and its expansion, rendered as standard output of the model, have been thoroughly studied in this work. The analyses of turbulence intensity reveals a clearly anisotropic pattern of the turbulence across the shear layer, particularly in the transition and far wake regions, which corroborates the need for an anisotropic turbulence treatment, as the one implemented herein. The spatial distribution of momentum turbulent diffusion is studied by performing a dimensionless correlation analysis. Different directional momentum transfer rates are obtained in the shear layer, the study of which enables for its stable location and expansion.

Unfortunately, experimental data regarding the velocity characteristics in the wake of the NedWind 46/3/500 turbine was not available at the time. Nevertheless, a qualitative comparison, with data available from measurements in the literature (Schlez et al, 2001; Barthelmie et al, 2004; Rados et al, 2001) was performed. It should be noted that when performing a qualitative comparison in the near wake region, there is an acceptable agreement between the obtained flow properties and the

experimental results reported in the previous single wake studies (Schlez et al, 2001; Barthelmie et al, 2004; Rados et al, 2001). However in the far wake region the present model appears to overestimate the velocity deficit values. This in turn, would lead to inaccurate estimation of the downstream distance needed for the full wake restoration. Operationally, it is worth mentioning that other approaches presented in the literature have experimented similar problems (Crespo et al, 1999). Results were improved by incorporating empirical laws for wake turbulence calculations purposes. This finding strongly suggests that the problem might be connected with the specific turbulence model. Moreover, as mentioned at describing the equations of the model, part of the constants, used at this stage, were taken as the default values given in the commercial software package (Fluent, 2001). Some of them have been obtained for flow patterns, for example homogeneous shear flows, which not necessarily fit with those relevant for the present problem. Future work is required in order to obtain physically verified values of the model constants and further explore this issue. Once the issue of the values of the relevant constants is cleared up, an additional inherent advantage of the model might be posed by its elliptic character, regarding the estimation of velocity deficit. In other words, since velocity deficit recovery, obtained by the accumulation of lateral momentum transfer along the axial direction is essentially a 2-D mechanism, the use of such treatment might have a naturally corrective effect.

In the light of the significant increase of computational capabilities available nowadays, the use of general models like the Reynolds stress model, offers a readily available tool for the improvement of this type of analysis. This improvement is evident in terms of investigating anisotropic properties and understanding the relevant full scale three dimensional wake flows. This would be particularly relevant in comparison with previous isotropic studies or tailored software which requires extensive programming efforts. Moreover, these computational capabilities make the realization of an analysis of this type for a limited group of turbines, a viable option.

Future work will include tuning of the model constants, in order to test the capabilities of the model to reproduce field measurements in the transition and far wake regions. Once the procedure would be completed, the model could be safely extended to a number of turbines in order to study their wake interactions. According to the experimental observations cited above (Vermeer et al, 2003; van Leuven, 1988) repeatability of the extracted power, beyond the second row in a turbine array is

obtained. The proposed numerical approach implemented for a small array, could then provide information relevant for wind farm design.

FIGURE CAPTIONS

Figure 1. Schematic picture of the wind turbine.

Figure 2. The computational domain.

Figure 3. Computational domain. Volumes assembly.

Figure 4. Typical mesh structure surrounding turbine blade.

Figure 5. Iso-curves (m/sec) of the velocity component in *x* direction: (a) in the vertical mid lengthwise section; (b) in the horizontal mid cross section**.**

Figure 6. Vorticity distribution in the mid horizontal cross section (x-y plane).

Figure 7. Velocity deficit distribution: (a) at different heights within the mid vertical lengthwise section (x-z plane); (b) at different downstream distances within the mid horizontal cross section (x-y plane); (c) at different downstream distances within the mid vertical lengthwise section (x-z plane).

Fig. 8. Turbulence intensity distribution in the mid vertical lengthwise section (x-z plane) at several downstream distances: (a) in the average flow (*x*) direction; (b) in the lateral (*y*) direction; (c) in the vertical (*z*) direction. Height measured from hub axis.

Figure 9. Dimensionless correlation of fluctuating velocities (x-z plane) in the near and far wake of the turbine: (a) $\overline{u'_x u'_z}/U_0^2$; (b) $\overline{u'_y u'_z}/U_0^2$; (c) $\overline{u'_x u'_y}/U_0^2$.

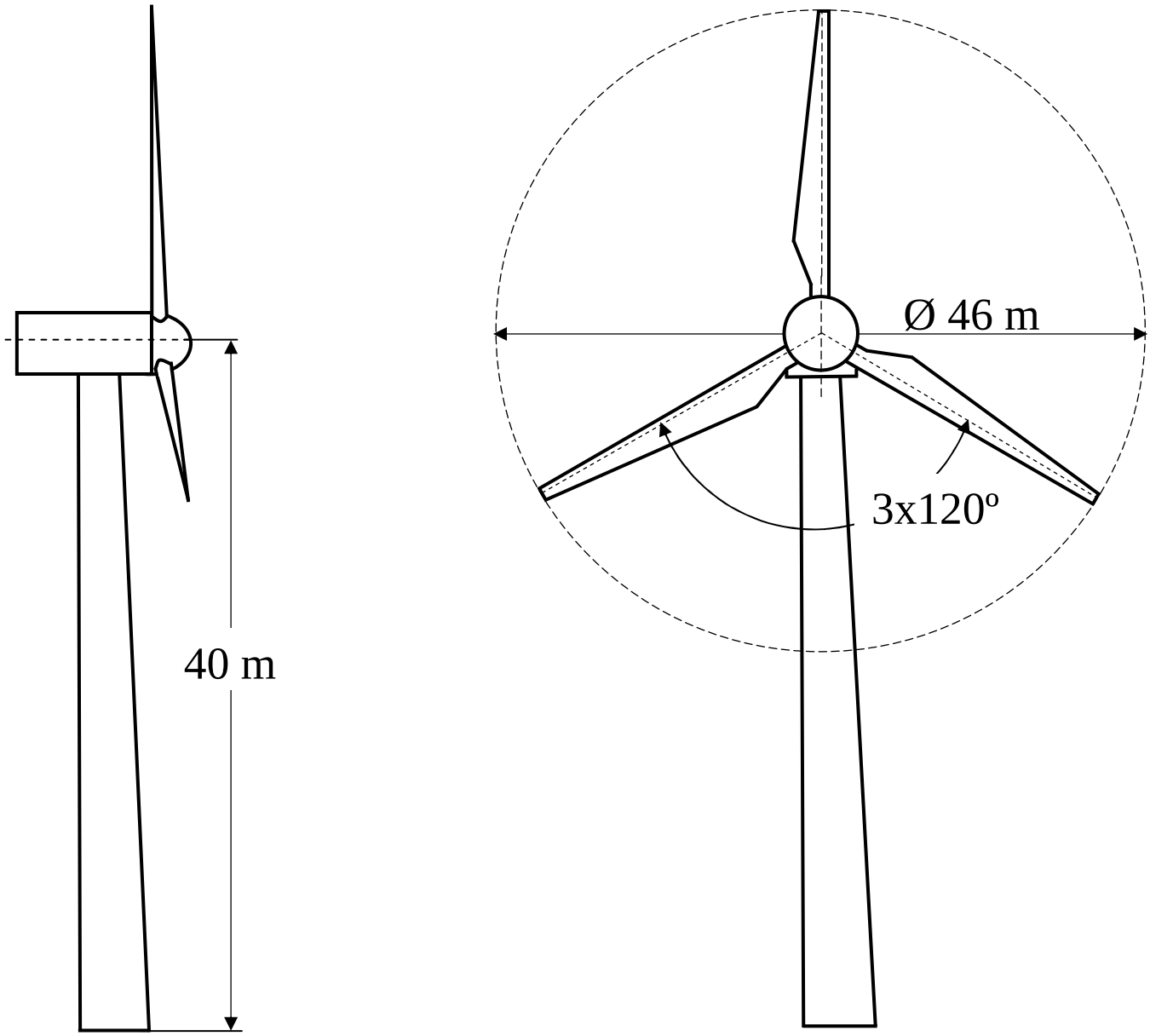

Fig. 1. Schematic picture of the wind turbine.

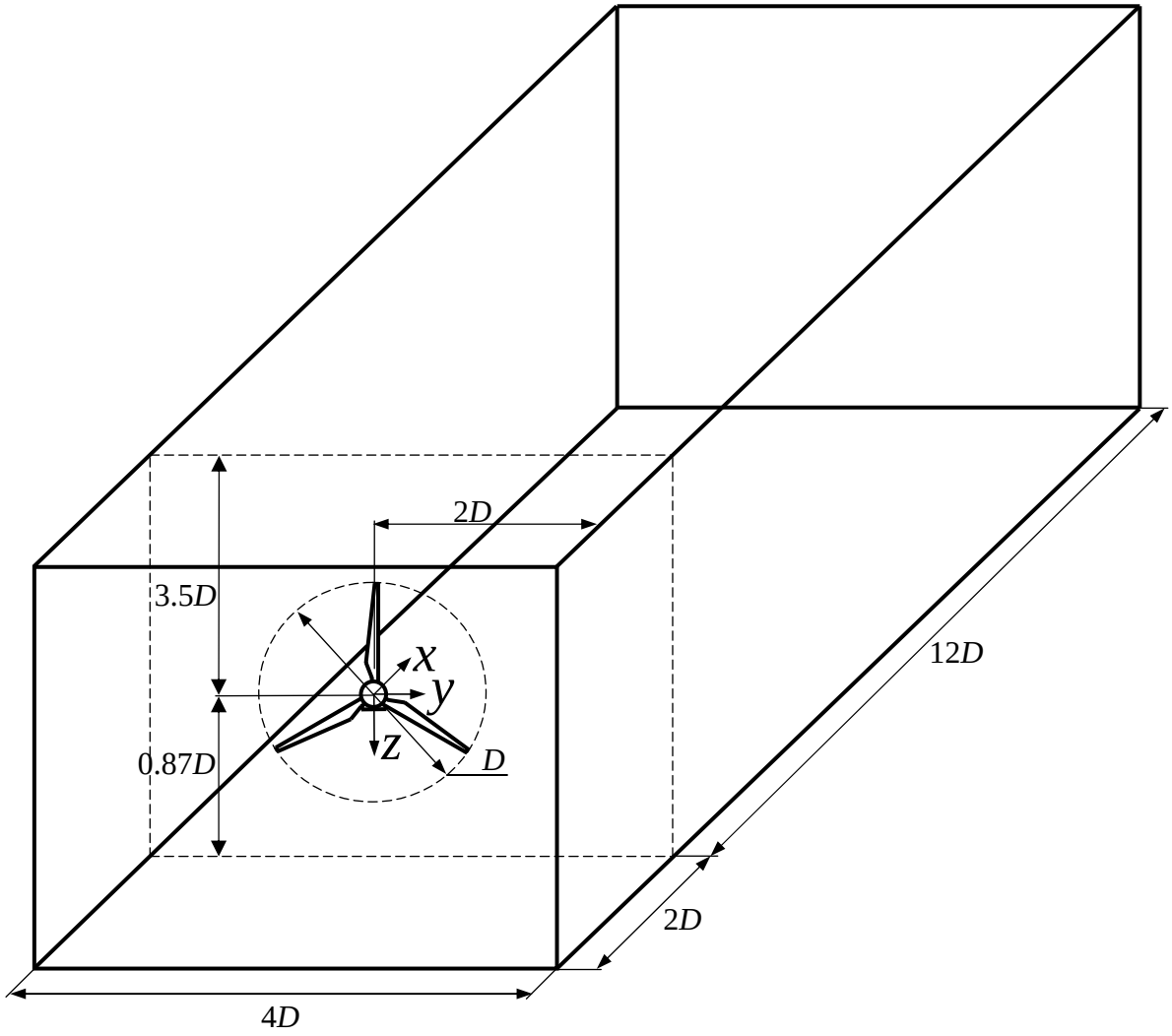

Fig. 2. The computational domain.

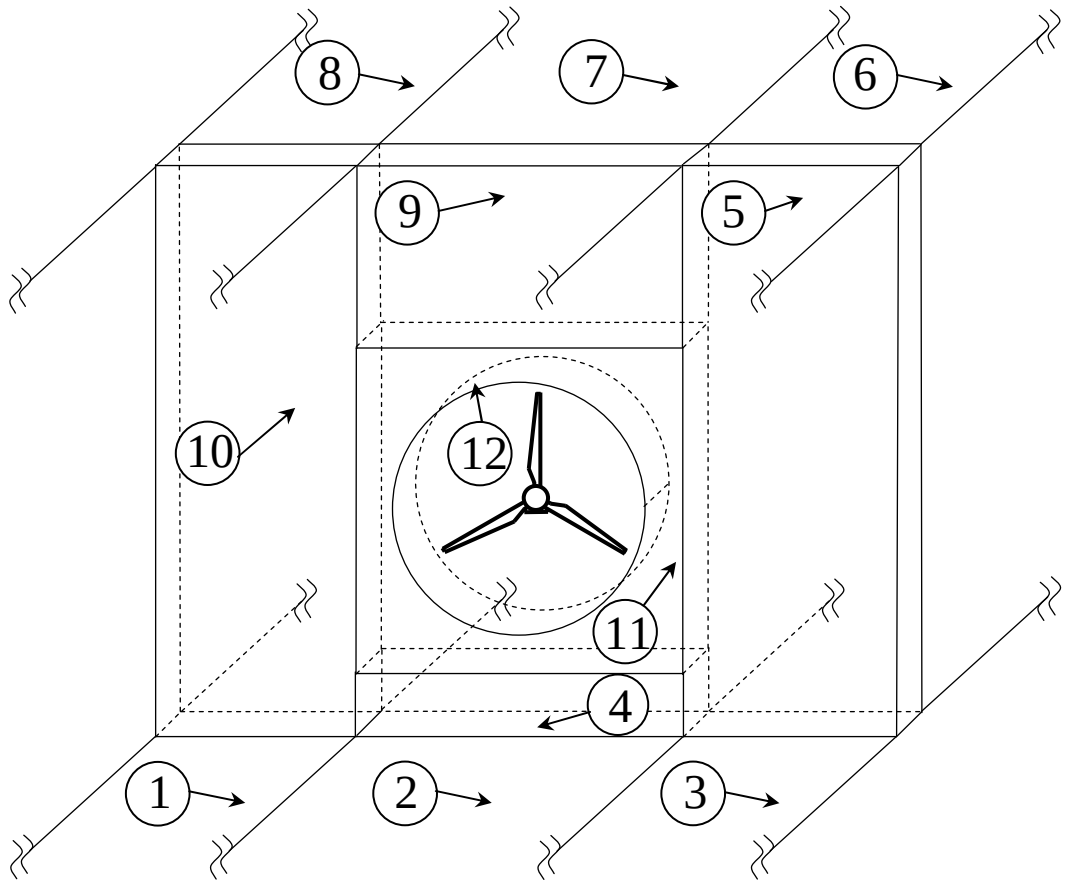

Fig. 3. Computational domain. Volumes assembly.

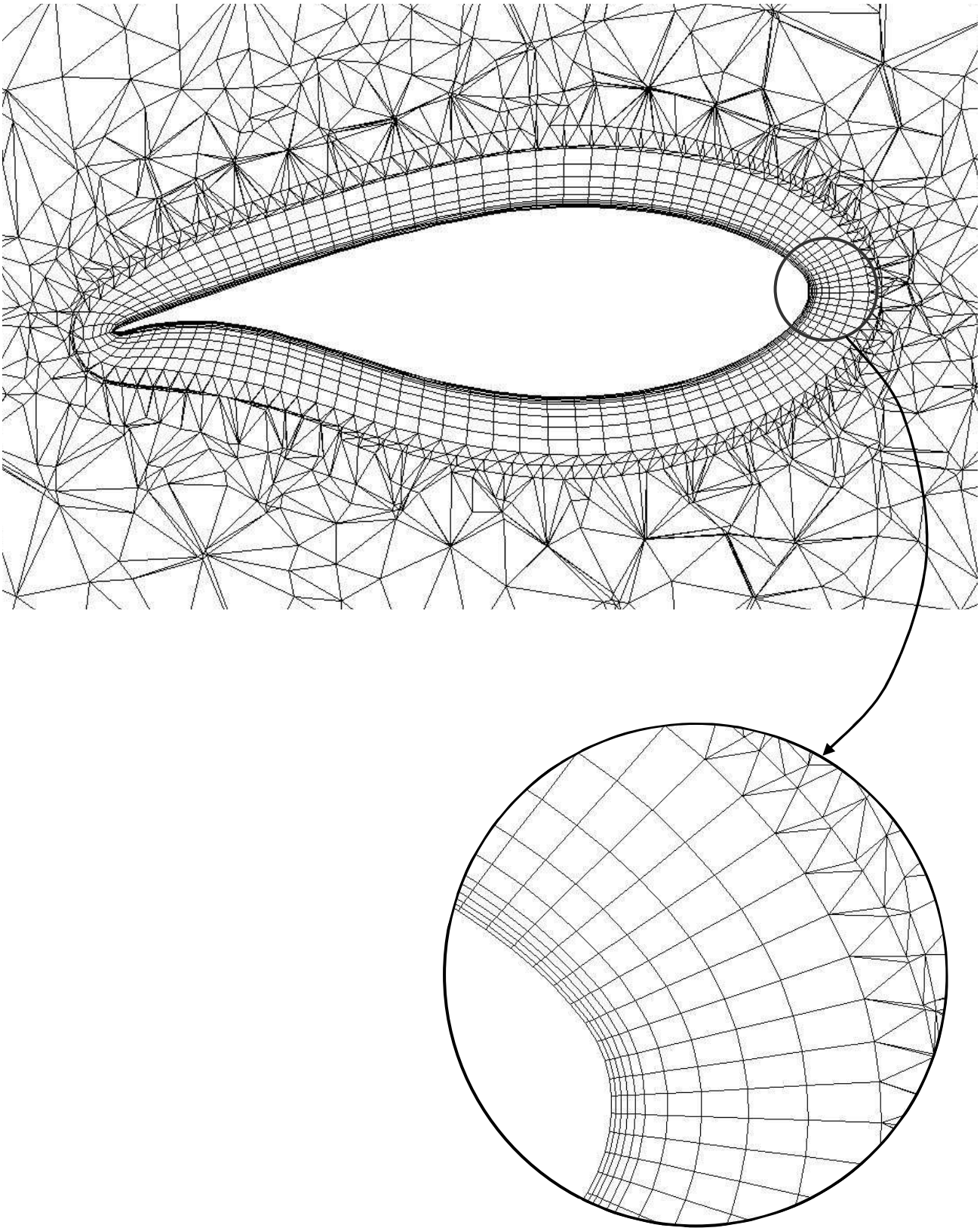

Fig. 4. Typical mesh structure surrounding turbine blade.

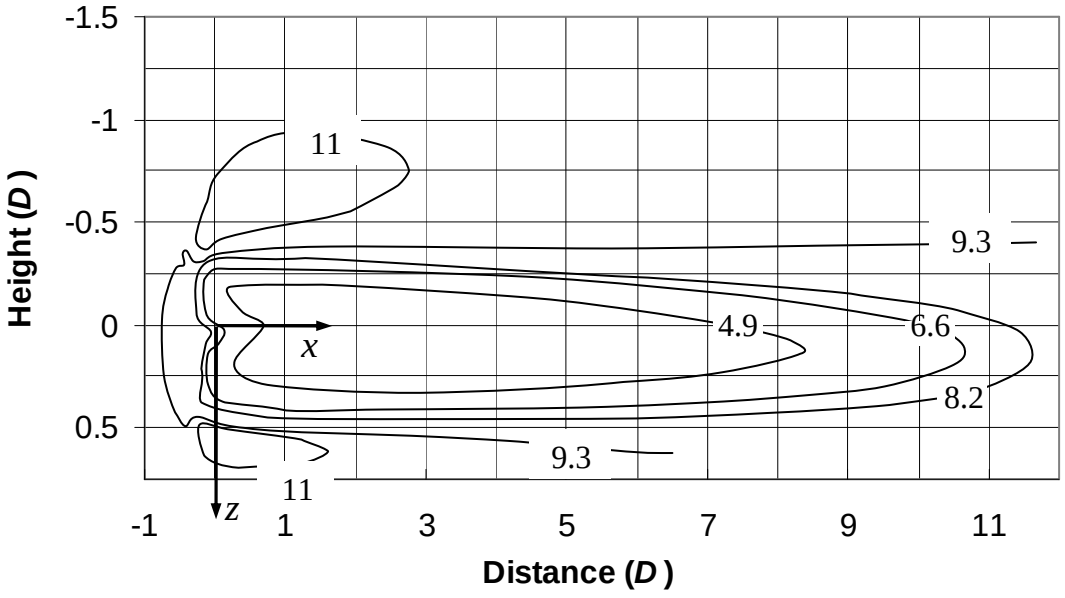

(a)

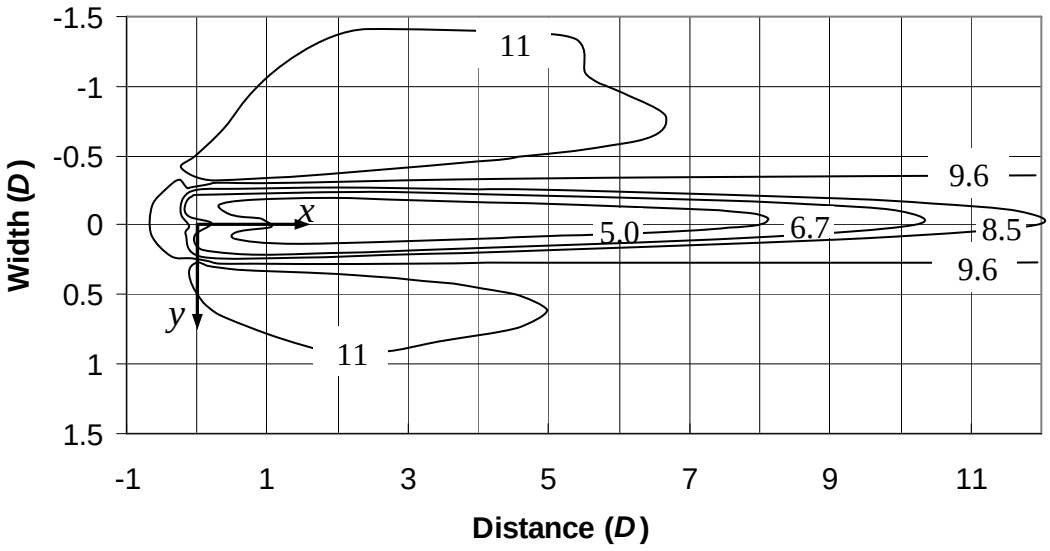

(b)

Fig. 5. Iso-curves (m/sec) of the velocity component in *x* direction: (a) in the vertical mid lengthwise section; (b) in the horizontal mid cross section.

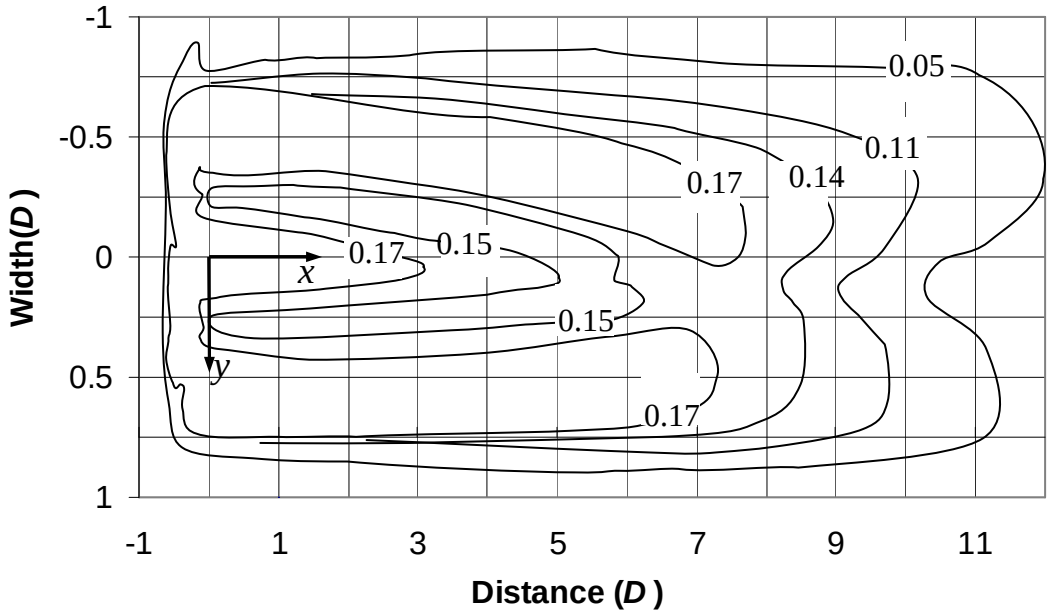

Fig. 6. Vorticity distribution in the mid horizontal cross section (x-y plane).

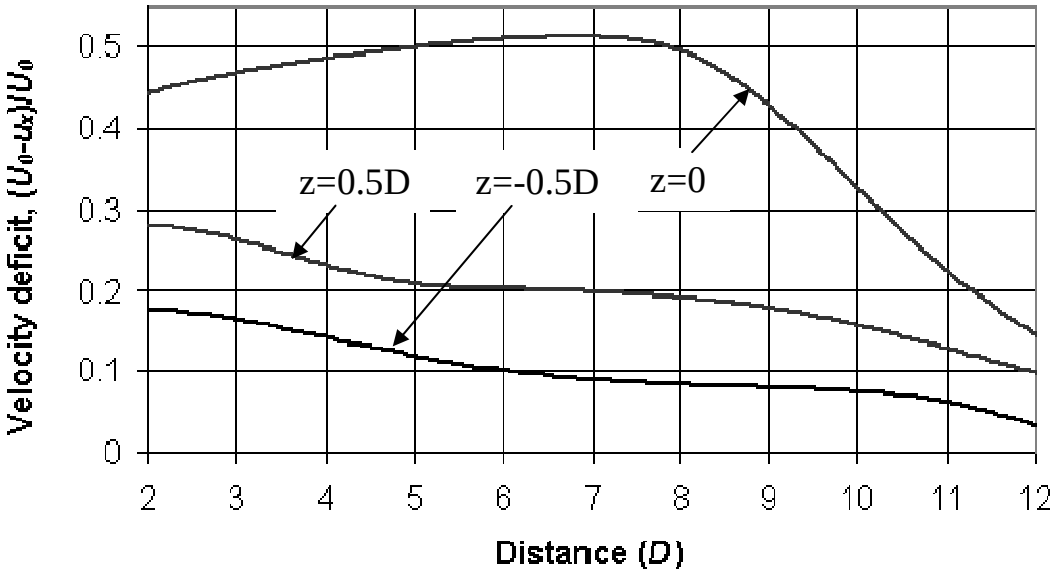
Velocity deficit, $(U_0-u_x)/U_0$
0.5
0.4
0.3
0.2
0.1
0
z=0.5D
z=-0.5D
z=0
2
3
4
5
6
7
8
9
10
11
12
Distance (D)

(a)

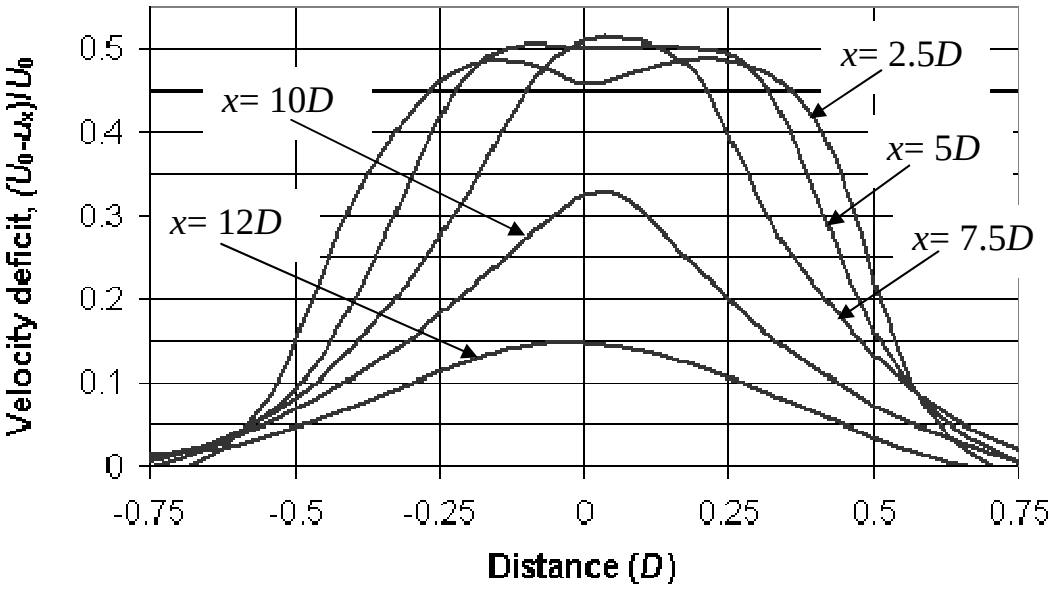
Velocity deficit, $(U_0-u_x)/U_0$
0.5
0.4
0.3
0.2
0.1
0
x= 2.5D
x= 10D
x= 5D
x= 12D
x= 7.5D
-0.75
-0.5
-0.25
0
0.25
0.5
0.75
Distance (D)

(b)

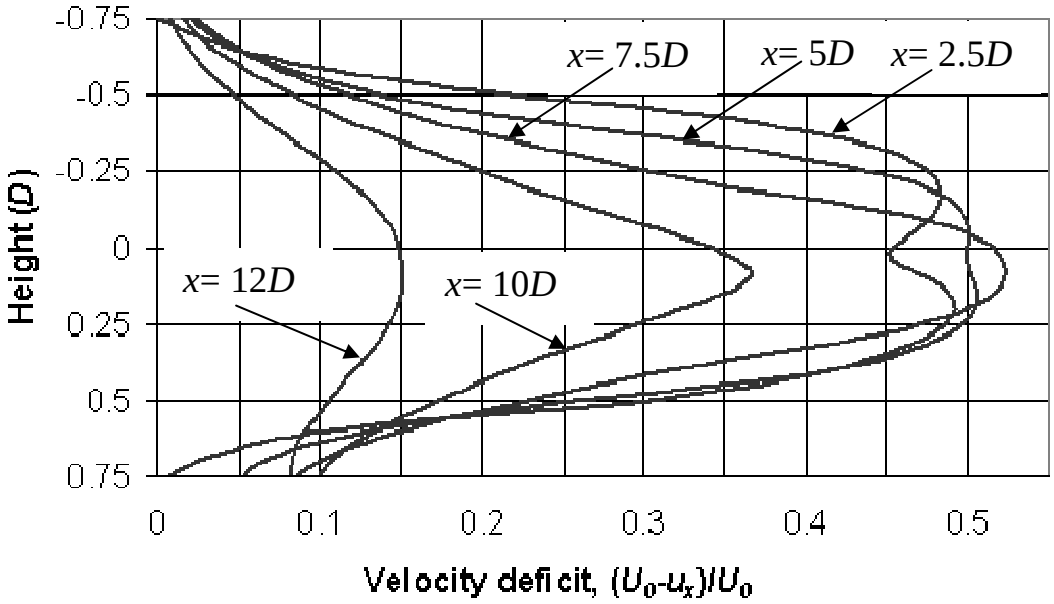

(c)

Fig. 7. Velocity deficit distribution: (a) at different heights within the mid vertical lengthwise section (x-z plane); (b) at different downstream distances within the mid horizontal cross section (x-y plane); (c) at different downstream distances within the mid vertical lengthwise section (x-z plane).

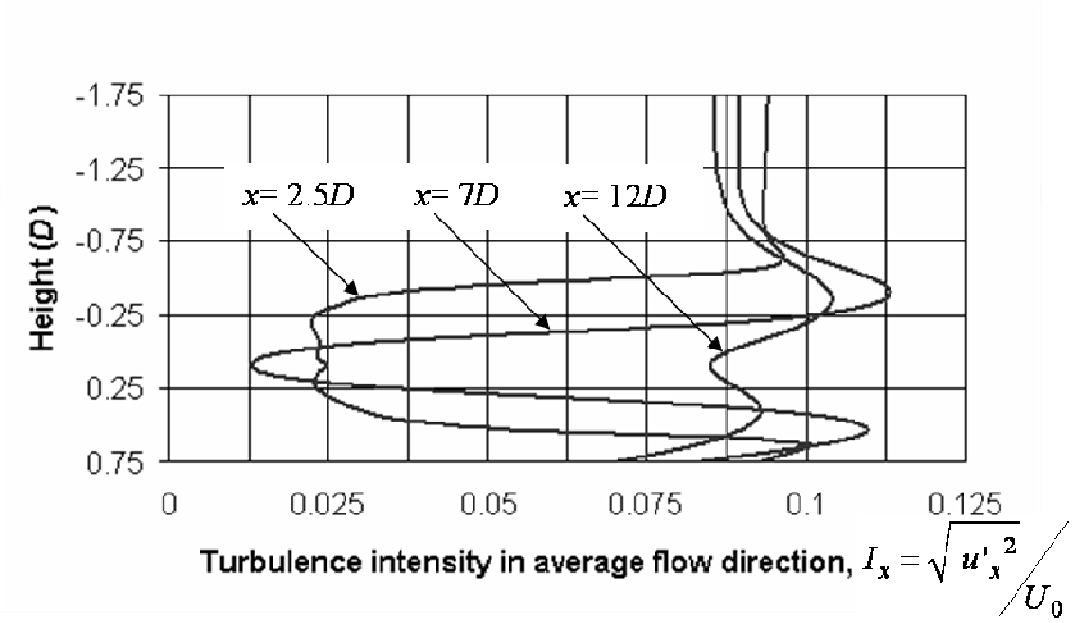
-1.75
-1.25
-0.75
-0.25
0.25
0.75
Height (D)
x= 2.5D
x= 7D
x= 12D
0
0.025
0.05
0.075
0.1
0.125
Turbulence intensity in average flow direction, $I_x = \sqrt{u'^2_x} / U_0$

(a)

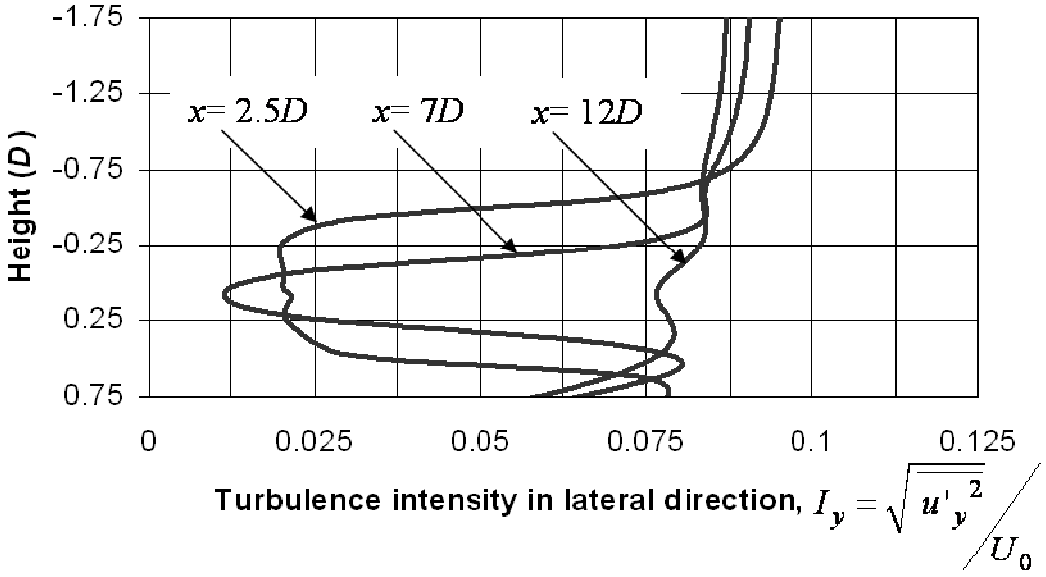
-1.75
-1.25
-0.75
-0.25
0.25
0.75
Height (D)
x= 2.5D
x= 7D
x= 12D
0
0.025
0.05
0.075
0.1
0.125
Turbulence intensity in lateral direction, $I_y = \sqrt{\overline{u'^2_y}} / U_0$

(b)

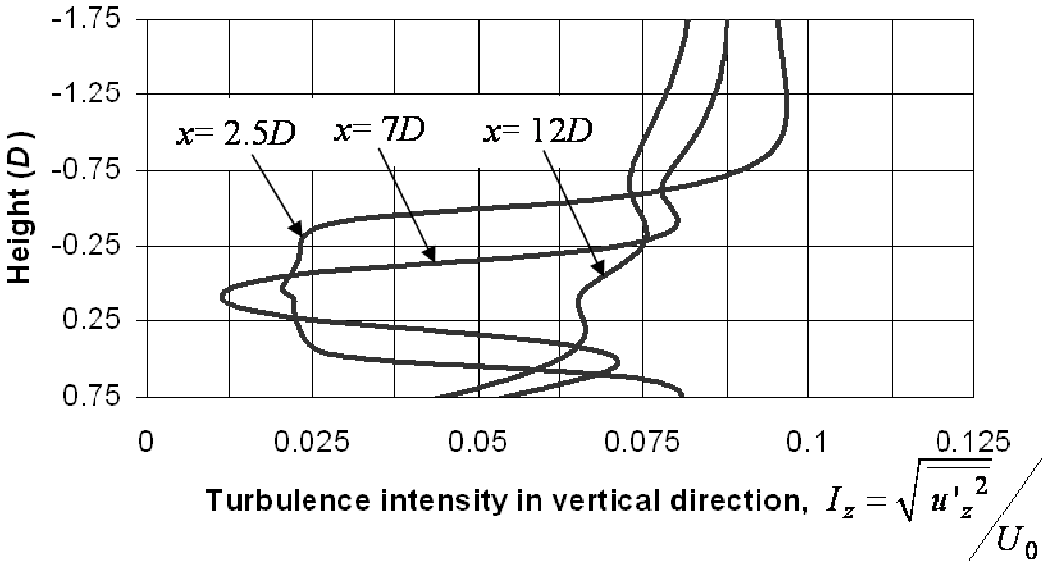

(c)

Fig. 8. Turbulence intensity distribution in the mid vertical lengthwise section (x-z plane) at several downstream distances: (a) in the average flow (*x*) direction; (b) in the lateral (*y*) direction; (c) in the vertical (*z*) direction. Height measured from hub axis.

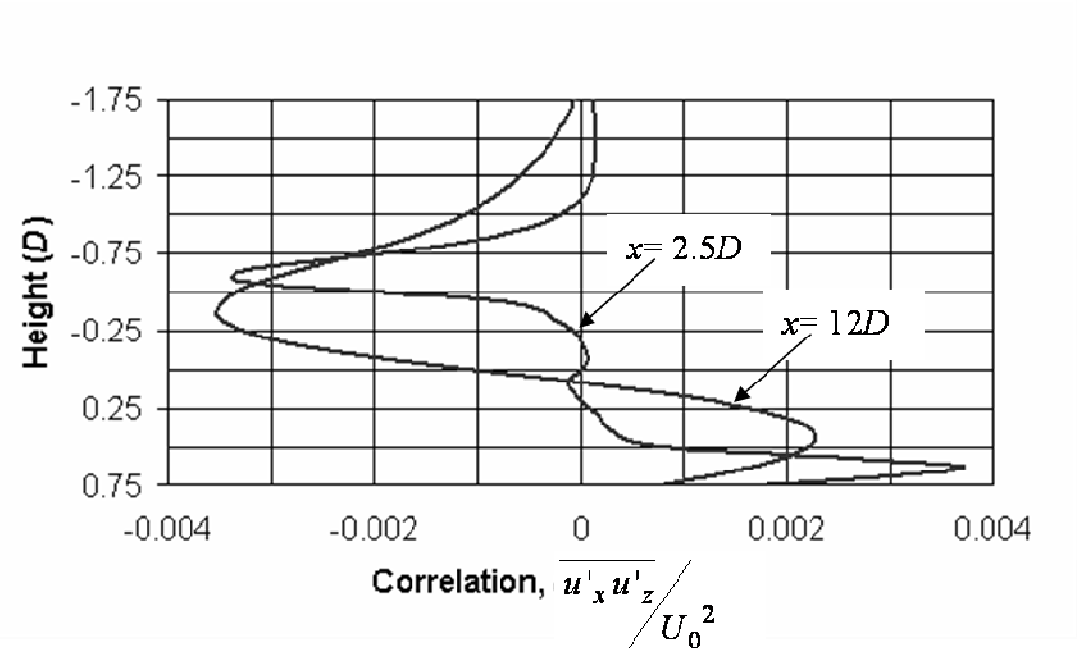
-1.75
-1.25
-0.75
-0.25
0.25
0.75
Height (D)
x= 2.5D
x= 12D
-0.004
-0.002
0
0.002
0.004
Correlation, $\overline{u'_x u'_z}/U_0^2$

(a)

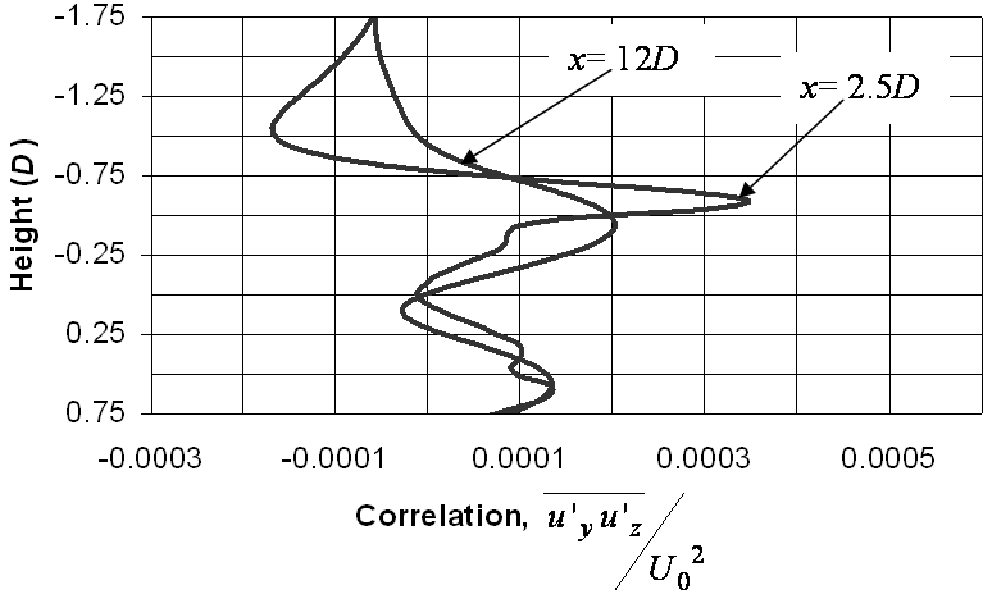
-1.75
-1.25
-0.75
-0.25
0.25
0.75
Height (D)
x= 12D
x= 2.5D
-0.0003
-0.0001
0.0001
0.0003
0.0005
Correlation, $\overline{u'_y u'_z}/U_0^2$

(b)

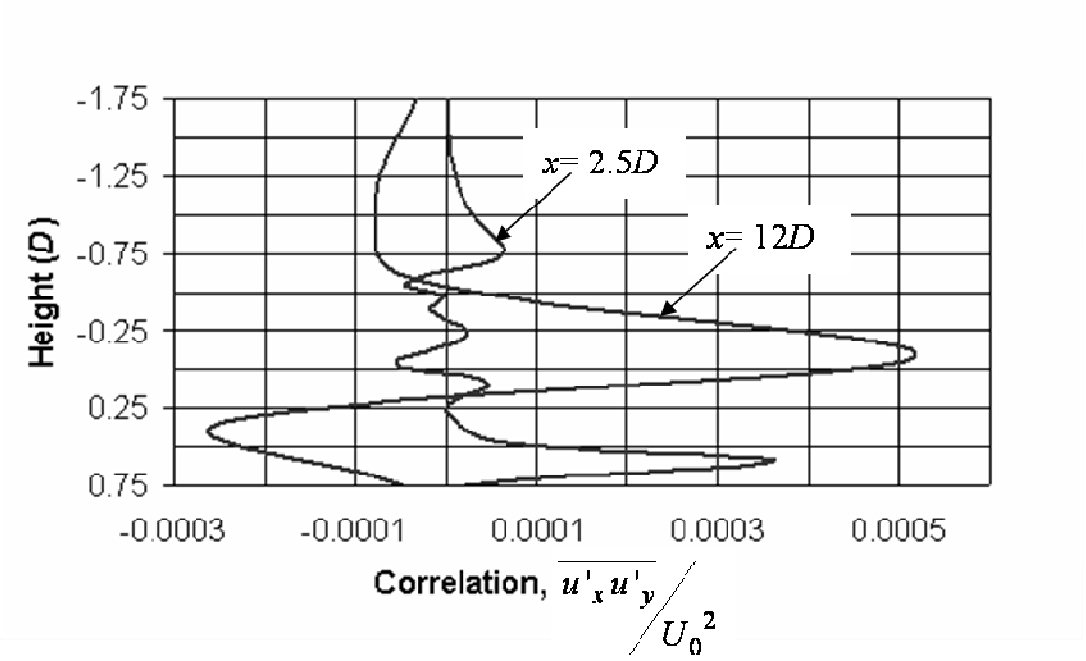

(c)

Fig. 9. Dimensionless correlation of fluctuating velocities (x-z plane) in the near and far wake of the turbine: (a) $\overline{u'_x u'_z}/U_0^2$; (b) $\overline{u'_y u'_z}/U_0^2$; (c) $\overline{u'_x u'_y}/U_0^2$.

References

Bak, C., Fuglsang, P., Sørensen, N.N., Madsen, H.A., 1999. Airfoil characteristics for wind turbines, Risø-R-1065(EN), Risø National Laboratory, Roskilde, Denmark.

Barthelmie, R., Larsen, G., Pryor, S., Jørgensen, H., Bergström, H., Schlez, W., Rados, K., Lange, B., Vølund, P., Neckelmann, S., Mogensen, S., Schepers, G. , Hegberg, T., Folkerts, L., Magnusson, M., 2004. ENDOW (Efficient development of offshore wind farms): Modeling wake and boundary layer interactions, Wind Energy 7, 225-245.

Beyer, H.G., Pahlke, T., Schmidt, W., Waldl, H.P., Witt, U., 1994. Wake effects in a linear wind farm. Journal of Wind Engineering and Industrial Aerodynamics 51, 303-318.

Corten, G.P., Schaak, P., Hegberg, T., 2004. Velocity profiles measured above a scaled wind farm, in: Proceedings of EWEC'2004, London, UK.

Crespo, A., Manuel, F., Hernandez, J., 1990. Numerical modeling of wind turbine wakes, in: Proceedings of the 1990 European Community Wind Energy Conference, Madrid, Spain, 166-170.

Crespo, A., Chacon, L., Hernandez, J., Manuel, F., Grau, J.C., 1994. UPMPARK: a parabolic 3D code to model wind farms, in: Proceedings of EWEC'94, Thessaloniki, Greece, 454-459.

Crespo, A., Hernandez, J., 1996. Turbulence characteristics in wind-turbine wakes. Journal of Wind Engineering and Industrial Aerodynamics 61, 71-85.

Crespo, A., Hernandez, J., Frandsen, S., 1999. Survey of Modeling Methods for Wind Turbine Wakes and Wind Farms. Wind Energy 2, 1-24.

Daly, B. J., Harlow, F. H., 1970. Transport equations in turbulence, Physics of Fluids, 13, 2634-2649.

Fluent 6 User's Guide, Fluent Inc., Lebanon, NH, 2001.

Fuglsang, P., Antoniou, I., Dahl, K. S., Madsen, H. A., 1998. Wind Tunnel Tests of the FFA- W3- 301 and NACA 63- 430 Airfoils. Riso- R- 1041 (EN), Riso National Laboratory, Roskilde.

Gomez-Elvira, R., Crespo, A., Migoya, E., Manuel, F., Hernandez, J., 2005. Anisotropy of turbulence in wind turbine wakes. Journal of Wind Engineering and Industrial Aerodynamics 93, 797-814.

Hinze, J.O., 1975. Turbulence, McGraw –Hill Publishing Co., New York.

Katic, I., HØjstrup, J., Jensen, N.O., 1986. A simple model for cluster efficiency, in: Proceedings of EWEC'86 , 407-410. International Solar Energy Society, Rome, Italy.

Lien, F. S., Leschziner, M. A., 1994. Assessment of turbulent transport models including non-linear RNG eddy-viscosity formulation and second-moment closure. Computers and Fluids, 23 (8), 983-1004.

Lissaman, P.B.S., 1979. Energy effectiveness of arbitrary arrays of wind turbines. AIAA Paper 79-0114, 1-7.

Magnusson, M., Rados, K.G., Voutsianas, S.G., 1996. A study of the flow downstream of a wind turbine using measurements and simulations. Wind Engineering 20(6), 389-403.

Magnusson, M., 1999. Near-wake behaviour of wind turbines. Journal of Wind Engineering and Industrial Aerodynamics, 80, 147-167.

Rados, K., Larsen, G., Barthelmie, R., Schlez, W., Lange, B., Schepers, G., Hegberg, T., Magnusson, M., 2001. Comparison of wake models with data for offshore windfarms. Wind Engineering 25 (5), 271-280.

Schlez, W., Umana, A., Barthelmie, R., Larsen, G., Rados, K., Lange, B., Schepers, G., Hegberg, T., 2001. ENDOW (Efficient development of offshore wind farms):

Improvement of wake models within offshore wind farms. Wind Engineering 25(5), 281-287.

Sørensen, J.N., Shen, W. Z., 2002. Numerical Modeling of Wind Turbine Wakes. J. Fluids Eng. 124 (2), 393-399.

Vermeer, L.J., SØrensen, J.N. Crespo, A., 2003. Wind Turbine Wake Aerodynamics. Progress in Aerospace Sciences 39, 467- 510.

van Leuven, J., Stevens, D., 1988. The wind farm of Zeebrugge: experimental set-up. Journal of Wind Engineering and Industrial Aerodynamics 27, 39-144.

Smith, D., Taylor, G.J., 1991. Further analysis of turbine wake development and interaction data, in: Proceedings of the 13th BWEA Wind Energy Conference, Swansea, UK, 325-331.